https://doi.org/10.5194/hess-2022-235
Preprint. Discussion started: 6 July 2022

Hydrology and Earth System Sciences
Discussions
Open Access

Machine-learning ensembled CMIP6 projection reveals socio-economic pathways will aggravate global warming and precipitation extreme

Piaoyin Zhang, Jianzhong Lu, Xiaoling Chen

State Key Laboratory of Information Engineering in Surveying, Mapping and Remote Sensing, Wuhan University, Wuhan, 430072, China

Correspondence to: Jianzhong Lu (lujzhong@whu.edu.cn)

https://doi.org/10.5194/hess-2022-235
Preprint. Discussion started: 6 July 2022

Hydrology and Earth System Sciences
Discussions
Open Access

Abstract: The climate change plays a key role in ecosystem evolution and has been proved to be affected by comprehensive factors including anthropogenic activities. The application of GCMs (General Circulation Models) launched by CMIP6 (Coupled Model Intercomparison Project Phase 6) has become a primary implement to catch future climate characteristics under different future socio-economic pathways. However, quantitative future climate change records with high credibility generated by robust GCMs merged datasets from CMIP6 are scarce. Most precious studies depended on traditional GCMs ensemble datasets (e.g., single, mean and medium) which were proved to be highly unstable. In this study, three machine learning methods (Ordinary Least Squares regression, Decision Tree, and Deep Neural Networks) were applied to ensemble temperature and precipitation from 16 CMIP6 GCMs simultaneously. Monthly optimal estimation of precipitation and temperature from three datasets were selected to generate a new ensemble dataset under three Socio-Economic Pathways (SSP1-2.6, SSP2-4.5 and SSP5-8.5). The new ensemble precipitation (temperature) dataset with the R=0.81 (0.99) is more accurate than all the single GCM. High credible analyses demonstrate that Europe and North America contribute more to global warming than Oceania, Africa and South America. The global continent break through 1.5 °C, 2 °C and 3 °C rising threshold in 2024, 2031 and 2048 under SSP5-8.5 scenarios. Most precipitation aggregates in July and August, while dry months fall in April and September to next February during the rest of 21st century. Global precipitation will be accelerated polarization with the decreasing trends of Africa and Asia ($p < 0.05$) under the scenario of SSP5-8.5. The proposed analysis provides credible opportunities and

https://doi.org/10.5194/hess-2022-235
Preprint. Discussion started: 6 July 2022

Hydrology and Earth System Sciences
Discussions

quantitative fundamental to understand future climate characteristics for ecology and meteorology.

1. Introduction

As essential components of global climate transformation, the pattern changes of temperature and precipitation broadly impact agricultural productivity (Iwamura et al., 2020; Ortiz-Bobea et al., 2021; Raupach et al., 2021), ocean acidification (Randall and van Woesik, 2015; Anthony, 2016), hydrological drought or flooding extremes (Zhang et al., 2019; Liu et al., 2021; Qi et al., 2021) and spreading viruses (Iwamura et al., 2020; Li et al., 2018), etc. The Paris Agreement was set for reinforcing global response to control warming level below 2 °C and pursuing for 1.5°C impact (Hulme, 2016; Schleussner et al., 2016) compared with the pre-industrial period (1850-1900). However, IPCC Sixth Assessment Report (AR6) statement has affirmed that emissions of greenhouse gases from anthropogenic activities are responsible for 1.1°C temperature rising if 1850-1900 is defined as the baseline period (IPCC, 2021). Hence, it is fundamental to predict climate characteristics depending on the robust projection data set for formulating future climate change policies.

The utilization of meteorological station data or satellite products is failed to project climate changes (Dar and Dar, 2021). However, the Coupled Model Intercomparison Project (CMIP) has provided a great number of GCMs (General Circulation Models) for researchers to catch future climate changes. In past decades, former CMIPs played

https://doi.org/10.5194/hess-2022-235
Preprint. Discussion started: 6 July 2022

an active role in regional studies which were related to climate change projection. Lee et al. (2020) indicated the rising of maximum precipitation in East Asia will exceed to 7, 15 and 35 percent under RCP2.6, RCP4.5 and RCP8.5 conditions at the end of the 21st century. Gaitán et al. (2019) employed 9 GCMs and demonstrated the greatest rising daily maximum temperature over Spain will reach to 7°C until 2100 for RCP8.5. In the 6th phase of CMIP, five Socio-Economic Pathways (SSPs) which launched to describe human development challenges (Iqbal et al., 2021; You et al., 2021; Xu et al., 2022; O'Neill et al., 2017). The resolution and dynamic parameterization scheme of models were also improved from CMIP5 to CMIP6 (Chen et al., 2021; Hamed et al., 2022). However, the findings generated by new ensemble climate global dataset are rarely reported under CMIP6 with the new emission strategy. Therefore, it is worthwhile to further utilize CMIP6 GCMs.

Due to physical parameters sensitivity of GCMs, model outputs perform unequally credible in a specific region or time. Climate change projection ignoring the temporal and spatial heterogeneity leads to the incredibility of the estimation. Utilizing only one model will improve the uncertainty of climate projection. Therefore, ensemble methods were widely used by taking advantage of multi GCMs. Currently, the application of ensemble models can be roughly divided into three categories: (1) use of individual models, average or medium combination and other traditional statistical methods with equivalent weights (Fu et al., 2020; Li et al., 2020; Narsey et al., 2020; Xin et al., 2020; Almazroui et al., 2021; Hermans et al., 2021), (2) new weighted

https://doi.org/10.5194/hess-2022-235
Preprint. Discussion started: 6 July 2022

procedures with spatiotemporal homogeneity, such as independence weighted mean (IWM) and multidimensional scaling (MDS) (Sanderson et al., 2015; Bai et al., 2021), (3) development of machine learning (ML) with nonlinear function to train selected models adjusted by bias correction (Xu et al., 2020; Wei et al., 2021).

Nowadays, ML applications in data-driven geoscience mainly focus on downscaling (Tran Anh et al., 2019; Vandal et al., 2019), land cover transmission (Condro et al., 2019; Gianinetto et al., 2020) and inversion model construction (Jiang et al., 2019a; Liu and Grana, 2019), etc. To correct climate models, ML has been proved to be an effective tool in taking advantage of excellent features from GCMs in several studies (Wei et al., 2021; Jose et al., 2022). Jose. et al. (2021) employed support vector machine in maximum temperature ensemble of CMIP GCMs with a slight improvement of R from 0.522 to 0.7. Kuma. et al. (2022) developed an ANN network to correct cloud feedback for CMIP5 dataset, which is superior to the mean ensemble approach, but ANN could only explain 47% variance. Though ML methods was successfully applied in the precious regional studies, regionalized models were just suitable for specified periods or regions (Singh et al., 2017). Mitra (2021) anticipated there were significant room for improvement of ML application in projection of climate variables with spatial-temporal heterogeneity consideration. The robust application of ML application in global climate projection based on CMIP6 GCMs is still limited and needs to be explored.

The study aims to investigate global future climate changes based on ensemble optimized climate datasets through ML. Firstly, the machine learning methods Ordinary Least Square (OLS), Decision Tree (DT), and Deep Neural Networks (DNN) were used to simulate historical global temperature and precipitation based on 16 individual GCMs. Then, the best monthly ensemble model would be selected to project temperature and precipitation (2015-2100) under SSP1-2.6, SSP2-4.5 and SSP5-8.5 scenarios. Finally, the tendency of global warming under 1.5℃, 2℃ and 3℃ was explored. The precipitation pattern on a global and continental scale also be identified under future scenarios. This study can provide scientific dataset support for scholars in related earth science research and offer predictable opinions on climate management measures for policy-makers.

2. Data and Methodology

2.1 Experimental data

2.1.1 Model outputs

In our study, monthly mean temperature and precipitation datasets were provided by CMIP6 GCMs output. Sixteen GCMs developed by 19 global institutions were selected as Table 1. The period of 1965-2014 and 2015-2100 were chosen for historical simulation and future SSPs-RCPs scenarios, respectively. Future climate change was projected under scenarios SSP1-2.6, SSP2-4.5 and SSP5-8.5 corresponding to the

https://doi.org/10.5194/hess-2022-235
Preprint. Discussion started: 6 July 2022

sustainable development pathway, central pathway following the historical pattern and fossil-intensive emission pathway (O'Neill et al., 2016), respectively. There are different grid sizes for the selected GCMs, therefore bilinear interpolation was applied to unify the resolution to 0.5°×0.5°.

Table 1 Detailed description of selected CMIP6 models

Model Name	Modeling group	Original
BCC-CSM2-MR	Beijing Climate Center, China / Meteorological Administration, China	1.125°×1.125°
CanESM5	Canadian Centre for Climate Modelling and Analysis, Canada	2.8125°×2.8125°
CESM2-WACCM	National Center for Atmospheric Research, Climate and Global Dynamics Laboratory, USA	1.25°×0.9375°
CMCC-CM2-SR5	Fondazione Centro Euro-Mediterraneo sui Cambiamenti Climatici Italy	1.25°×0.9375°
CMCC-ESM2	Fondazione Centro Euro-Mediterraneo sui Cambiamenti Climatici,Italy	1.25°×0.9375°
FGOALS-f3-L	Chinese Academy of Sciences, China	1.25°×1°
INM-CM4-8	Institute for Numerical Mathematics, Russia	2°×1.5°
INM-CM5-0	Institute for Numerical Mathematics, Russia	2°×1.5°
KACE-1-0-G	National Institute of Meteorological Sciences/Korea Meteorological Administration, Republic of Korea	1.875°×1.25°
MIROC6	The University of Tokyo, National Institute for Environmental Studies, and Japan Agency for Marine–Earth Science, Japan	1.4063°×1.4063°
MRI-ESM2-0	Meteorological Research Institute, Japan	1.125°×1.135°
NESM3	Nanjing University of Information Science and Technology, China	1.875°×1.875°
TaiESM1	Research Center for Environmental Changes, Taiwan	1.25°×0.9375°
MPI-ESM1-2-HR	Max Planck Institute for Meteorology, Germany	0.9375°×0.9375°
MPI-ESM1-2-LR	Max Planck Institute for Meteorology, Germany	0.9375°×0.9375°

https://doi.org/10.5194/hess-2022-235
Preprint. Discussion started: 6 July 2022

FIO-ESM-2-0	FIO (First Institute of Oceanography, State Oceanic Administration, China), QNLM (Qingdao National Laboratory for Marine Science and Technology, China)	1.25°×0.9375°

2.1.2 Observation datasets

High resolution (0.5° × 0.5°) CRU TS4.05 grids (Das et al., 2016) were obtained as monthly observation dataset for mean temperature and precipitation. Compared with previous CRU TS4.0, the latest version CRU TS4.05 covered more complete time series (Jan. 1901- Dec. 2020) was provided by the University of East Anglia in July 2021(Ullah et al., 2020). Considering the time-series matching problem and premature period lack of reliability, data during period (Jan.1965- Dec.2014) were used to simulate and validate multi-model ensemble results.

2.2 Multi-model ensemble methods

In the processing of multi-model ensemble, CRU TS4.05 and 16 GCMs was chosen as ground truth and simulation dataset. Period encompassing 1965-2014 was spilt into training period (1965-1994) and testing period (1995-2014). The input datasets are 5760 GCMs images and 540 observation images, and each image consists of 67420 pixels (Fig.1). In the training process of ensemble methods, OLS (Ordinary Least Squares regression), DT (Decision Tree) and DNN (Deep Neural Networks) were applied to optimize the monthly dataset.

https://doi.org/10.5194/hess-2022-235
Preprint. Discussion started: 6 July 2022

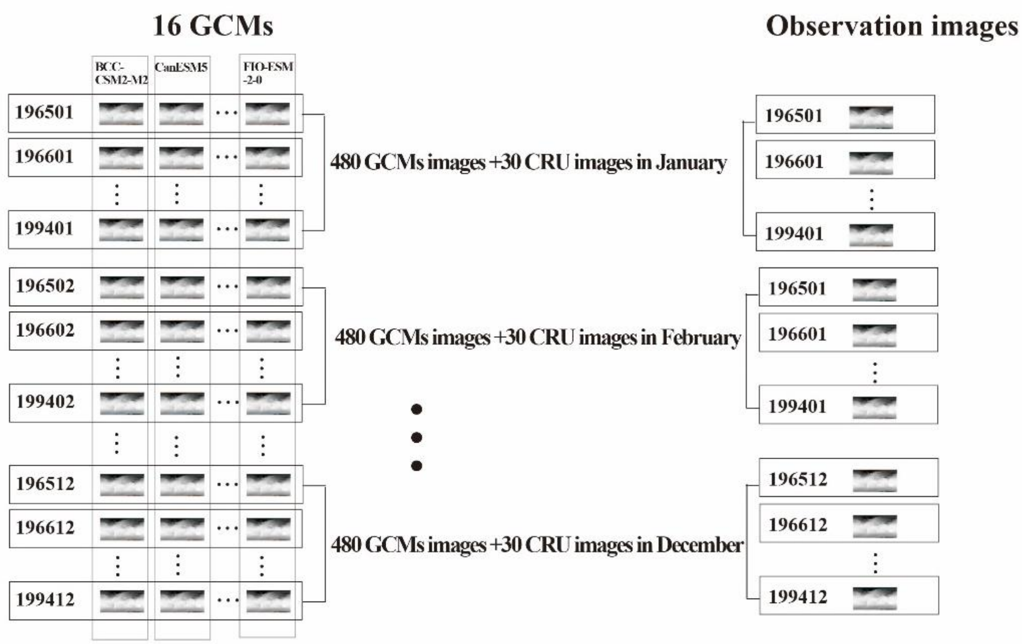

Fig. 1. Weight assignment of 16 GCMs on a time scale

The Ordinary Least Squares regression (OLS) is a widely technique applied for estimating the unknown coefficients of linear regression equations which determine the relationship between one or more independent quantitative variables and another variable (Lee et al., 2022). To construct the optimization function, OLS aims to minimize the sum of squared residuals between observed and predicted data (Sharif et al., 2017). The OLS method was employed to assign weights for 16 selected GCMs with linear regression at the monthly scale. The weight matrix generated by OLS can be expressed as follow.

$$\begin{bmatrix} W^1 \\ W^2 \\ \vdots \\ W^i \\ \vdots \\ W^{12} \end{bmatrix} = \begin{bmatrix} \beta_1^1, & \beta_2^1, & \cdots, & \beta_j^1, & \cdots, & \beta_{16}^1, & \varepsilon_1 \\ \beta_1^2, & \beta_2^2, & \cdots, & \beta_j^2, & \cdots, & \beta_{16}^2, & \varepsilon_2 \\ \vdots & \vdots & \vdots & \vdots & \vdots & \vdots & \\ \beta_1^i, & \beta_2^i, & \cdots, & \beta_j^i, & \cdots, & \beta_{16}^i, & \varepsilon_i \\ \vdots & \vdots & \vdots & \vdots & \vdots & \vdots & \\ \beta_1^{12}, & \beta_2^{12}, & \cdots, & \beta_j^{12}, & \cdots, & \beta_{16}^{12}, & \varepsilon_{12} \end{bmatrix} \quad (1)$$

https://doi.org/10.5194/hess-2022-235
Preprint. Discussion started: 6 July 2022

where β_j^i represents the weight of the j^{th} GCM in the i^{th} month; ε_i represents the residual generated after weight distribution for i^{th} month.

To obtain ensemble value of each pixel, the linear model generated by OLS can be described as follow.

$$Y^{(i,k)} = \sum_{p}^{i=1} \beta_j^i X_j^{(i,k)} + \varepsilon_i \tag{2}$$

where $Y^{(i,k)}$ and $X_j^{(i,k)}$ denote the values of single k^{th} pixel value in the ensemble image and the image of j^{th} GCM, respectively.

The DT method is usually applied to construct a nonlinear model which is sensitive to intermediate missing values with stronger explanatory than linear regression (Pekel, 2020). According to the training input dataset, each region is recursively divided into two subregions originally, in which the output value is determined to construct a binary decision tree (Jumin et al., 2021). The process can be described as four steps in details:

Step 1: Each GCM represents a dimension of a space. Dividing the j^{th} dimension of the space into two regions (R1 and R2) by selected candidate splitting the j^{th} GCM as the feature, and then splitting the pixel values into two groups as following equations.

$$\mathrm{R1}(\mathrm{j},\mathrm{s}) = \{\mathrm{x} \mid \mathrm{x}(\mathrm{j}) \leq \mathrm{s}\} \tag{3}$$

$$\mathrm{R2}(\mathrm{j},\mathrm{s}) = \{\mathrm{x} \mid \mathrm{x}(\mathrm{j}) > \mathrm{s}\} \tag{4}$$

Step 2: Adjusting the j and s to minimize the residual sum of squares following equation 4.

https://doi.org/10.5194/hess-2022-235
Preprint. Discussion started: 6 July 2022

$$min_{j,s}\left[min_{c_1}\sum_{x_i\in R_1(j,s)}(y_i-c_1)^2+min_{c_2}\sum_{x_i\in R_2(j,s)}(y_i-c_2)^2\right] \quad (5)$$

$$c_m=\frac{1}{N_m}\sum_{y_i\in R_1(j,s)}y_i\ (x\in R_m, m=1,2) \quad (6)$$

where N_m is the total number (30 images × 67420 pixel/images) of observation data at current node; y_i is the i^{th} individual sample of observation data.

Step 3: Repeating steps 1 and 2 to continue increasing the depth of tree and splitting the subregions R1 and R2 until training loss reaches to criteria threshold. Mean-absolute-error was applied as supported criteria to measure the quality of a split in this study.

The Deep Neural Network (DNN) is a feedforward artificial neural network, which is applied to explore the relationship between input features and construct linear equations for ground truth. It is an effective strategy to solve supervision problems (classification, regression, clustering, etc.) (Raheli et al., 2017; Jiang et al., 2019b). In this study, DNN can be split into three parts: 1input layer, 3 hidden layers and 1 output layer, meanwhile the output of each hidden layer is transformed by the ReLU activation function. To obtain the optimal weight of selected 16 GCMs on time scale, DNN is needed to construct for each month. In the process of training, the method adjusts the parameters, or the weights and biases of the model to minimize error. Our DNN neural network was designed (Fig. 2) with 0.001 learning rate. Input $Node_i$ represents the pixel values in the images of i^{th} GCM in the form of vector [$pixel_1$, $pixel_2$, …, $pixel_m$]. Output Node represents the pixels in the images of ensemble images in the form of vector [$pixel_1$,

https://doi.org/10.5194/hess-2022-235
Preprint. Discussion started: 6 July 2022

Hydrology and Earth System Sciences
Discussions

pixel$_2$, …, pixel$_m$]. Supposing there are m and n neurons in the k^{th} and $(k+1)^{th}$ layers, respectively, the output weight a^k of the k^{th} layer can be described as follow.

$$a^k = W^k a^{k-1} + b^k \tag{7}$$

where b^k represents $1 \times n$ residual vector; W^k represents a $n \times m$ weight matrix composed of linear coefficient of the k^{th} layer.

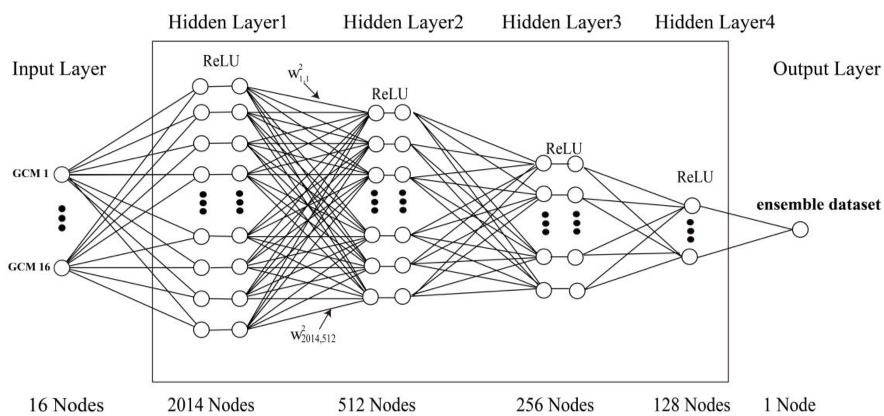

Fig. 2. Main Deep Neural Networks structure constructed in study. $\omega^{l}_{j,k}$ represents the weight from the j^{th} neuron in the $(l-1)^{th}$ layer to the k^{th} neuron in the l^{th} layer.

2.3 Model performance assessment

The statistic indices including correlation coefficient (*R*), centralized root mean square difference (CRMSE), standard deviation (SD) ratio and mean absolute error (MAE) are employed to quantify the loss between simulation and observation data. The comprehensive rating index was applied to assess the overall result performance.

Correlation coefficient (*R*) ranging from -1 to 1 is employed to determine the linear

https://doi.org/10.5194/hess-2022-235
Preprint. Discussion started: 6 July 2022

relationship between variables. According to R, correlation strength can be divided into five degrees (Asuero et al., 2006), representing very strong ($0.7 < |R| \leqslant 1$), strong ($0.5 < |R| \leqslant 0.7$), moderate ($0.3 < |R| \leqslant 0.5$), weak ($0 < |R| \leqslant 0.3$) and none ($|R| = 0$) relationships, respectively. Positive R denotes variables moving in same direction and negative R represents variables move in opposite direction. The most widely applied coefficient was generated by the Pearson product-moment correlation. R is calculated as follows (Maimon et al., 1986):

$$R = \frac{\sum_{i=1}^{n}(x_i - m_x)\left(y_i - m_y\right)}{\sqrt{\left[\sum_{i=1}^{n}(x_i - m_x)^2\right]\left[\sum_{i=1}^{n}\left(y_i - m_y\right)^2\right]}} \quad (8)$$

where x_i, y_i are the values of x and y for the i^{th} individual; m_x, m_y denote mean value of compared variables x and y, respectively; n denotes pairs of observation and model data matched by time-interspace.

The CRMSE and SD ratio are constructed as following equations (Taylor, 2001):

$$\text{CRMSE} = \sqrt{\frac{1}{n}\sum_{i=0}^{n}\left[(x_i - m_x) - \left(y_i - m_y\right)\right]^2} \quad (9)$$

$$\text{SD ratio} = \frac{\sqrt{\sum_{i=1}^{n}(x_i - m_x)^2}}{\sqrt{\sum_{i=1}^{n}(y_i - m_y)^2}} \quad (10)$$

All parameters in Equation 3 and 4 have the same meaning as Equation 2.

To evaluate the accuracy of the given model, mean absolute error (MAE) was proposed with range of 0 to $+\infty$. The lower the value of MAE, the better a model fits the dataset, where 0 suggests perfect simulation capability. MAE can be expressed as follows:

https://doi.org/10.5194/hess-2022-235
Preprint. Discussion started: 6 July 2022

Hydrology and Earth System Sciences Discussions Open Access EGU

$$MAE = \frac{1}{N}\sum_{i=1}^{N}|y_o - y_p| \tag{11}$$

where y_o and y_p represent the individual of original and predicted values, respectively; N denotes the number of observed individuals.

The assessment results of best single models or ensemble methods using different evaluation indicators will be different. Therefore, Comprehensive Rating Index (CRI) restricted in 0 to 1 is devised to unify standards to normalize simulation capabilities and give concise overall ranking summary of 16 studied single models and 3 ensemble methods (Jiang et al., 2015). The performance with CRI close to 1 is proved to be suitable. CRI can be computed by the following formula:

$$\mathrm{CRI} = 1 - \frac{1}{i\,j}\sum_{p=0}^{i} rank_p \tag{12}$$

where i and j denote the number of evaluation indices and investigated models or methods, respectively; rank_p denotes the rank of model or method according to p^{th} index.

3. Results

3.1 Accuracy validation of proposed dataset by observation data in historic period

3.1.1 Accuracy assessment of monthly averaged precipitation and temperature with Taylor diagram

To illustrate the accuracy of 16 GCMs and 3 ensemble methods, Taylor diagram was applied to integrate R, SD ratio and CRMSE measurements (Fig. 2). The best optimal

https://doi.org/10.5194/hess-2022-235
Preprint. Discussion started: 6 July 2022

performance is equipped with the lowest CRMSE, highest R and SD ratio closing to 1 in Taylor diagram. Obviously, the accuracy of OLS and DNN results was better under historical scenarios than precipitation or temperature from each GCM (Fig. 3a). Despite slightly more excellent performance in temperature, DT method was far superior to other single models with a significantly higher *R* of 0.71 against CRU TS4.05 precipitation under validation period (1995-2014). The SD ratio of 16 models and 3 methods were all closed to 1 while R exceeded to 0.95. The DNN method owned the perfect simulation with the highest *R* of 0.985 and lowest CRMSE of 0.171 mm/month, followed by the OLS method (R=0.983, CRMSE=0.181 mm/month) and the DT method (R=0.972, CRMSE=0.232 mm/month). The R and CRMSE of single model ranged from 0.956-0.971 and 0.247-0.298 mm/month. Compared with the CanESM5 model ranked as the poorest model, the DNN method reduces CRMSE by 42.7%. In terms of precipitation (Fig. 3b), R of the OLS, DT and DNN methods were 0.800, 0.718 and 0.819, larger than other single models with a range of 0.541-0.654, respectively. R indicated that the simulation result produced by ensemble methods owned higher credibility. The results accuracy ranked in top three with CRMSE were still datasets from ensemble methods DNN (CRMSE = 0.601) > OLS (CRMSE = 0.619)> DT (CRMSE = 0.827).

https://doi.org/10.5194/hess-2022-235
Preprint. Discussion started: 6 July 2022

Hydrology and Earth System Sciences
Discussions

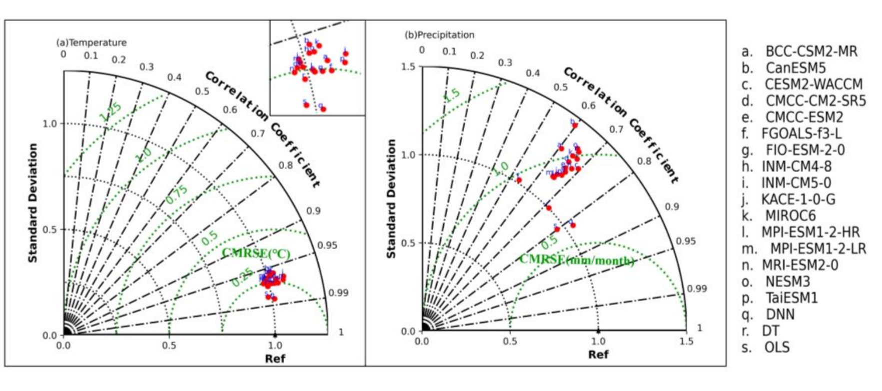

Fig. 3. Taylor diagrams of (a) temperature and (b) precipitation. Ref stands for CRU TS4.05 observation dataset

3.1.2 Accuracy assessment by spatial pattern of MAE

To further verify the simulation performance of the single models and ensemble methods, MAE was employed as another evaluation criterion. The value of MAE closer to 0 indicated more precise simulation. The quantitative results were shown in Fig.4 where red lines denoted median MAE and blue lines represented mean MAE. In terms of temperature and precipitation, the ranks of performance determined by mean MAE were both DNN > OLS > DT > any selected single model. Moreover, median MAE of the DNN and OLS method were 18.3 mm/month and 18.7 mm/month (1.88 ℃ and 1.96 ℃) in projecting precipitation (temperature), which showed significant robustness of both methods.

https://doi.org/10.5194/hess-2022-235
Preprint. Discussion started: 6 July 2022

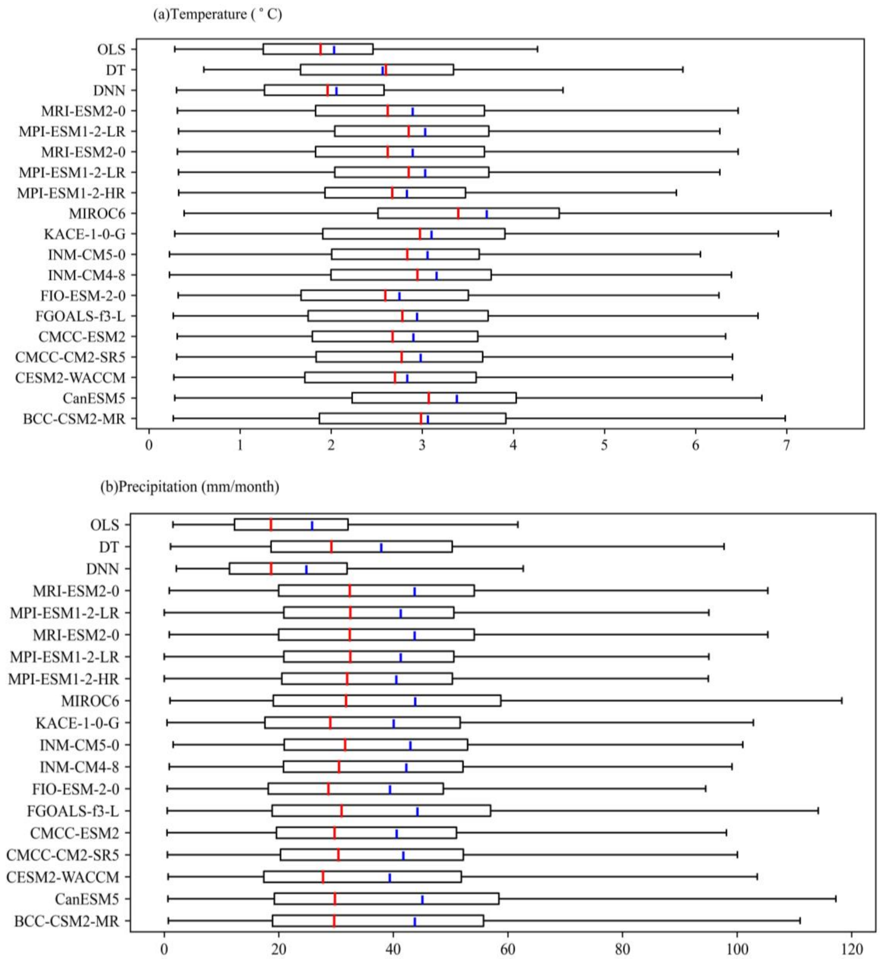

Fig. 4. Boxplots of Quantitative MAE assessment between simulation and observation dataset for (a) temperature (°C) and (b) precipitation (mm/month). The statistical distribution of data was displayed based on a five-divided category (minimum, first quartile, median, third percentile and maximum).

As for temperature, MAE corresponding to each pixel (0.5°×0.5°) was mapped in Fig 5. According to the simulative mechanism, figures can be divided into two groups: Fig5(a)-(p) and Fig5(q)-(s). The former revealed MAEs produced by 16 single models, the latter suggested MAEs processed by ensemble methods. For 16 GCMs, with the

https://doi.org/10.5194/hess-2022-235
Preprint. Discussion started: 6 July 2022

increase of latitude in the northern hemisphere, the area ratio with red gradually increased, which implies the upper regions of the northern hemisphere owned higher density of MAE. Estimation in the southern hemisphere is far better than the northern hemisphere. Evidently, the projection each single model was far inferior to ensemble methods. Compared with a single model, the OLS, DT and DNN methods reduced MAE in the northern hemisphere. For example, it is obvious that the tendency of MAE from 16 GCMs to ensemble methods decreased in Siberian plain, which locates in the middle and high latitudes with significant continental climate. The extremely low temperature in Siberian plain is only second to Antarctic continent, which leads to the increasing challenge of climate change projection. There were still minor defects in the sub-regions of the Andes Mountains in South America. The quality of the dataset generated by different ensemble methods largely depends on the input GCMs, which is the reason for the shortcomings in above mentioned area.

A similar MAE assessment is also conducted to precipitation. Contrary to temperature, MAE performance of precipitation was more excellent in the northern hemisphere than in the southern hemisphere (Fig. 6). In addition, the error showed an upward tendency with latitude increasing in the south hemisphere. It is undeniable that ensemble methods significantly mitigated the gap between observation and simulated gridded data especially in southeastern Asia continent (Indian Peninsula, the Tibetan Plateau, Thailand, etc.). Forecasts near the Andes Mountains were still unsatisfactory in precipitation. Lack of accuracy in single model greatly amplified the difficulty of

https://doi.org/10.5194/hess-2022-235
Preprint. Discussion started: 6 July 2022

Hydrology and Earth System Sciences
Open Access
Discussions

climate change projection.

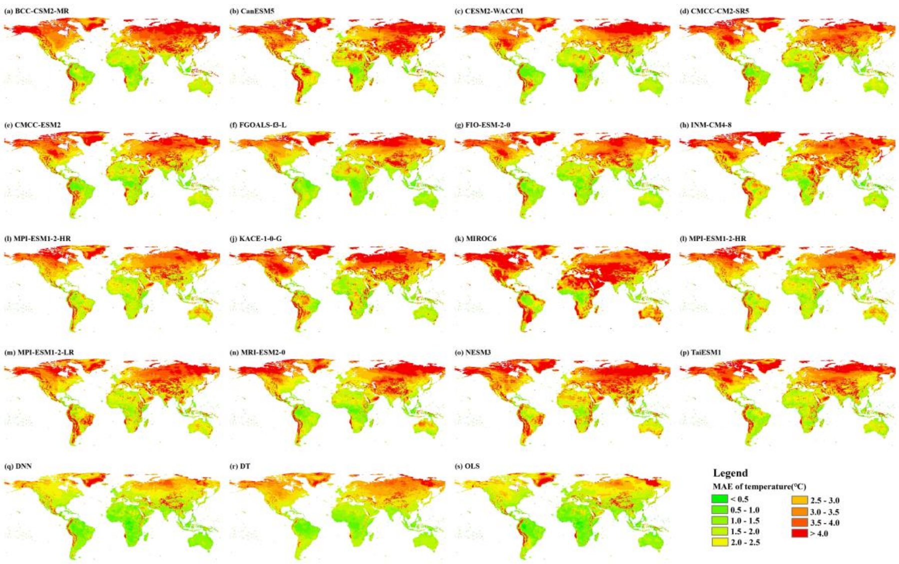

Fig. 5. The spatial distribution illustration of temperature MAE produced by selected CMIP6 models, DNN (Deep Neural Networks), DT (Decision Tree), and OLS (Ordinary Least Squares regression).

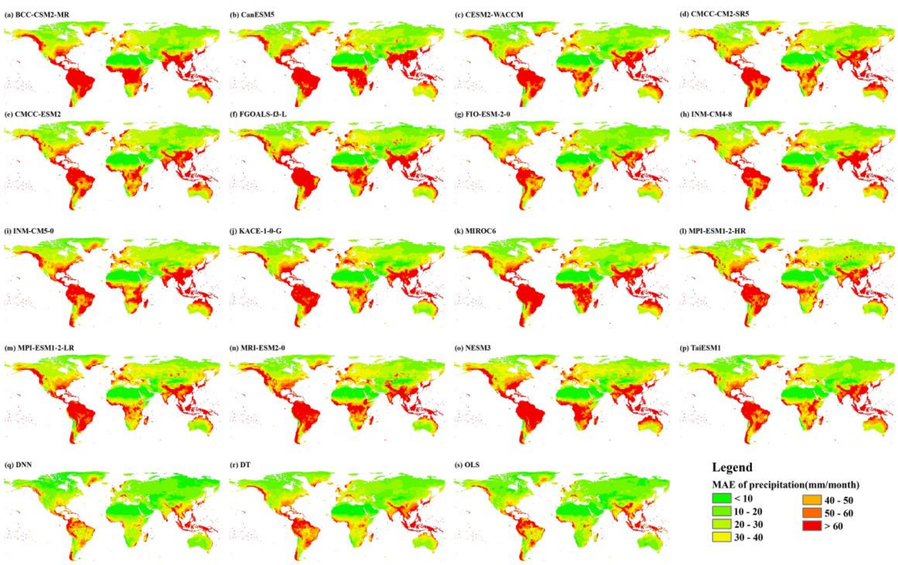

Fig. 6. The spatial distribution illustration of precipitation MAE produced by selected CMIP6 models, DNN (Deep Neural Networks), DT (Decision Tree) and OLS (Ordinary Least Squares regression

https://doi.org/10.5194/hess-2022-235
Preprint. Discussion started: 6 July 2022

Hydrology and Earth System Sciences Discussions

3.1.3 Overall performance evaluation

Due to the partial model assessment of a single indicator, different metrices result in different ranks. it is necessary to employ comprehensive index to improve the credible evaluation. To further measure superiority of different models, different monthly index rankings were calculated firstly before CRI assessment. The closer the pixel color to green, the better the ranking is, vice versa. Each pixel in heatmaps of CRI ranking (Fig 6) was calculated by four indices (R, CRMSE, SD ratio and MAE) according to the monthly ranking of single model and ensembled dataset. What cannot be ignored is that the proposed datasets from three ML methods ranked ahead of CRI generated by four indicators with green covered ribbons in both temperature (Fig 7.a) and precipitation prediction (Fig 7.b). Particularly, the DNN method was the optimal one among investigated single model and multi-model ensembled datasets. As for temperature, R values for the DNN methods were all ranked first for all months. Results from the DNN method ranked at 1 according to the CRMSE and MAE in each month except February, in which it ranked at 2.

The precipitation dataset from the DNN method ranked 1 in all months according to the MAE. The ranks with indicator R and CRMSE were either first or second indicating stable and perfect performance of DNN. Based on the SD ratio, results from the DNN method ranked middle. However, the SD ratio represented the overall pattern between the observation and simulation instead of the corresponding relations sample by sample.

https://doi.org/10.5194/hess-2022-235
Preprint. Discussion started: 6 July 2022

Hydrology and Earth System Sciences
Discussions
Open Access

Therefore, the SD ratio was not regarded to be persuasive compare with other indicators.

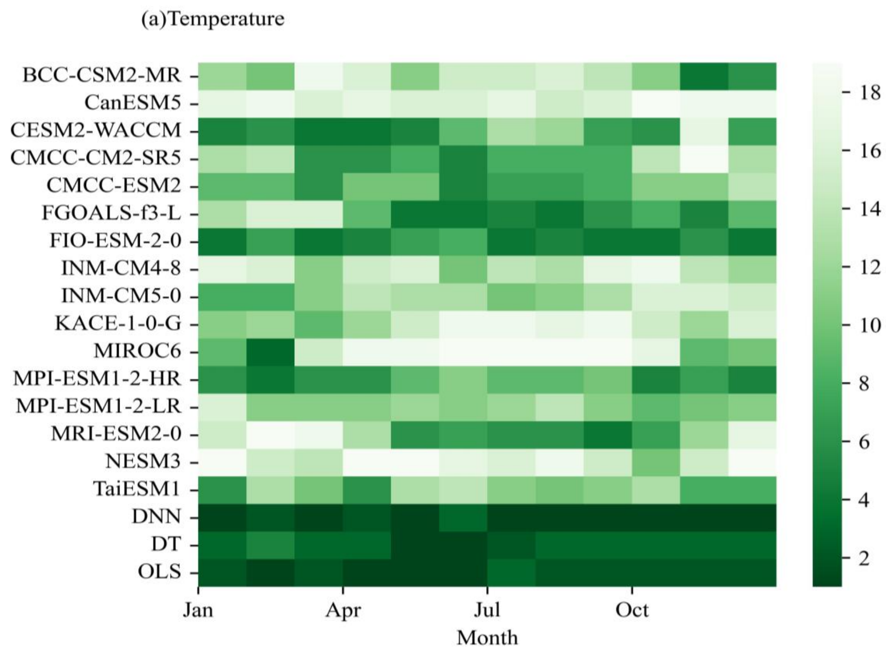

Hydrology and Earth System Sciences
Open Access
Discussions

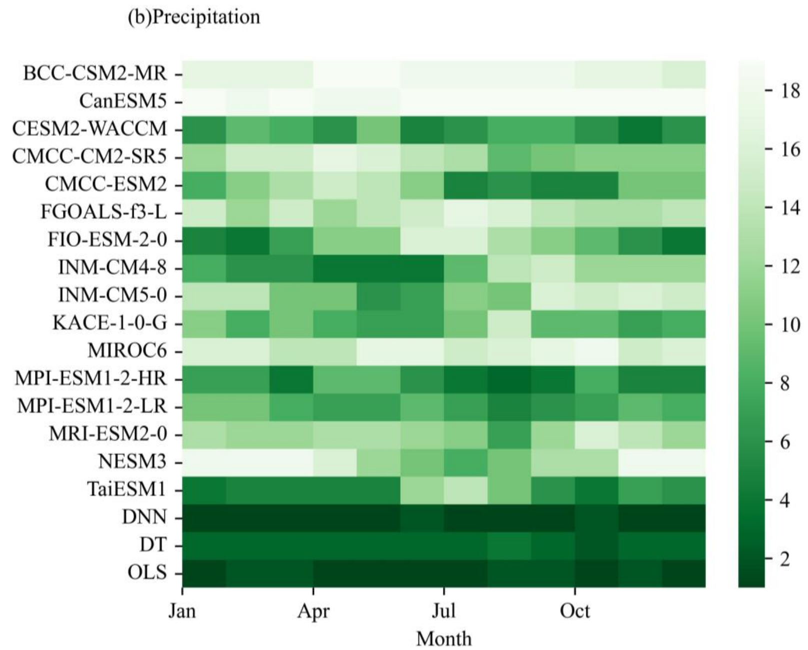

Fig. 7. CRI ranking of 16 single models and datasets from three ML methods. (a) temperature and (b) precipitation.

According to the CRI ranking results, the monthly optimal pattern was screened out to produce the new optimal dataset. In summary, the DNN method had an overwhelming advantage in all months except in February and April, in which the OLS method was the optimal method for temperature ensemble. On the other hand, the OLS was the best method for projecting precipitation from March to June and October, meanwhile the DNN produced optimal results in other months. Notably, there were two or more optimal methods in certain months (e.g., March, May) due to the same CRI ranking produced by the discrepancy of the partial indicator. Considering the stability, robustness, and R representing fitting ratio, the DNN method was employed as the optimal method for further predictive analysis when facing above situation.

https://doi.org/10.5194/hess-2022-235
Preprint. Discussion started: 6 July 2022

3.2 Years projection for temperature increasing under the 1.5℃ (2℃ / 3℃) global warming target

From the proposed optimal monthly dataset, temperature was projected under SSP1-2.6, SSP2-4.5 and SSP5-8.5 scenarios for the period of 2015-2100. As well, the pre-industrial period (1850-1900) dataset from CMIP6 was selected as reference to years projection for temperature increasing under the 1.5℃ (2℃ / 3℃) global warming target. For further intuitive analysis of temperature anomalies, global studied area was divided into Asia, Africa, Europe, South America and North America and Oceania continents. The temperature trends were shown in Figure 8. Clearly, the upward trend of SSP1-2.6 was steadier while steepest upward trend of the SSP5-8.5. What's more, Asia, Europe and North America continents contributed more to global warming than Oceania, Africa and South America continents in both scenarios.

The following simulated data are processed by 5-year moving average. In order to further confirm the time period of temperature rise in the study area, the rising targets of 1.5 ℃, 2 ℃ and 3 ℃ were set in Figure 8. Under the SSP1-2.6 scenario, Asia, Africa, South America, Oceania and global reach 1.5 ℃ threshold in the year of 2031, 2050, 2034, 2072 and 2037, respectively. Europe and North America continents get to 2℃ rising level during 2027 to 2029. If future followed the medium emission scenario namely SSP2-4.5, the years for Africa, South America and Oceania continents breakthrough 1.5 ℃ (2℃ / 3℃) warming target were 2024 (2037/2075), 2026 (2043/2082) and 2029 (2038/2094). Asia reached 3 ℃ warming target in 2026-2031

https://doi.org/10.5194/hess-2022-235
Preprint. Discussion started: 6 July 2022

and Europe reached 2 ℃ (3 ℃) level in 2026 (2040). Asia will firstly reach the 3 ℃ warming level, while Oceania continent is last one. The time breakpoints exceeding 1.5 ℃, 2 ℃ and 3 ℃ thresholds were 2029, 2035 and 2058 under the SSP2-4.5 scenario in global scale. the SSP5-8.5 scenario was denoted fossil-fueled development socioeconomic pathway. Therefore, it is not surprised to find the severity of temperature rising is greater than SSP 2-4.5 scenario. Under the SSP5-8.5 scenario, the time periods for global continent breakthrough 1.5 ℃, 2 ℃ and 3 ℃ rising threshold were 2024, 2031 and 2048, respectively. The period for Asia, Africa, Europe, South America and North America and Oceania continents for 3 ℃ warming target were 2024, 2055, 2036, 2031, 2060 and 2062 under the SSP5-8.5.

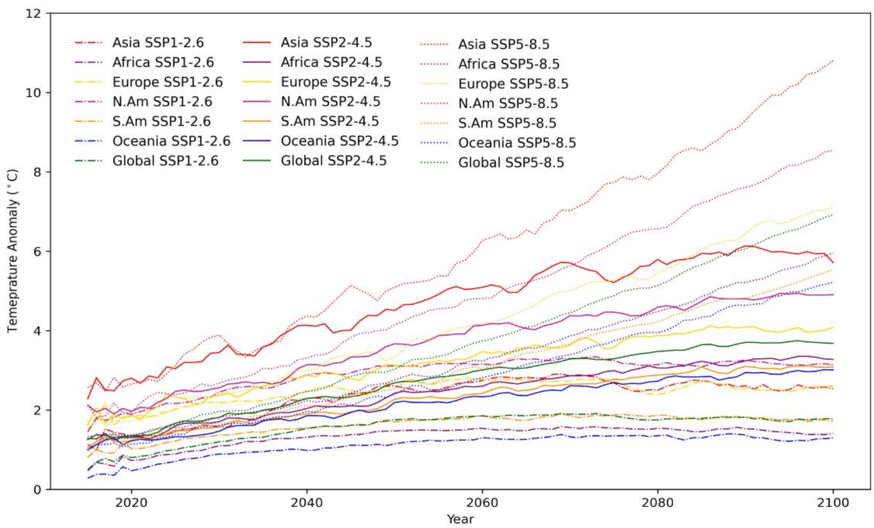

Fig. 8. Temperature anomalies of global and continents under (a) SSP1-2.6 (b) SSP2-4.5 and (c) SSP5-8.5 respect to pre-industrial temperature (1850-1900). N. Am denotes North America. S. Am denotes South America.

3.3 Tracking global and continental future precipitation changes

Monthly precipitation projection from 2015-2100 under three main scenarios were

https://doi.org/10.5194/hess-2022-235
Preprint. Discussion started: 6 July 2022

analyzed in Fig. 9 and Fig. 10. As the color bar shown, the closer color of the cell is bright red, the ampler the precipitation is. On the contrary, the closer the color is to green, the absent the precipitation is. In this study, we defined the spring (March to May), summer (June to August), Fall (September to November) and Winter (December to next February) in both north and south hemispheres to facilitate consistent analysis for different climate zones.

The tendency in intra-annual precipitation keeps rising under SSPs except for the decreasing tendency of winter under SSP1-2.6 (Fig. 9). From 2020-2100, July and August can be classified as wet months. On the other hand, April and September to next February can be categorized as dry months. In detail, summer rainfall is the most abundant. The amounts of summer value account for 31.6%, 29.1% and 29.8% of annual rainfall with the increase rates of summer at 0.30 mm/10a, 0.16 mm/10a and 0.76 mm/10a under SSP1-2.6, SSP2-4.5 and SSP5-8.5. Although the monthly precipitation in summer rank first in three selected scenarios, the increased monthly rainfall slopes of autumn, which can be determined as the peak among above SSPs, are 0.28 mm/10a, 0.63 mm/10a and 1.418 mm/10a under SSP1-2.6, SSP2-4.5 and SSP5-8.5, respectively. In terms of SSPs, the monthly wetter tendency of SSP5-8.5 is the most significant with a rate of 1.14 mm/10a. However, it doesn't mean that more uniform global precipitation distribution in all continents will happen.

https://doi.org/10.5194/hess-2022-235
Preprint. Discussion started: 6 July 2022

Hydrology and Earth System Sciences
Discussions
Open Access

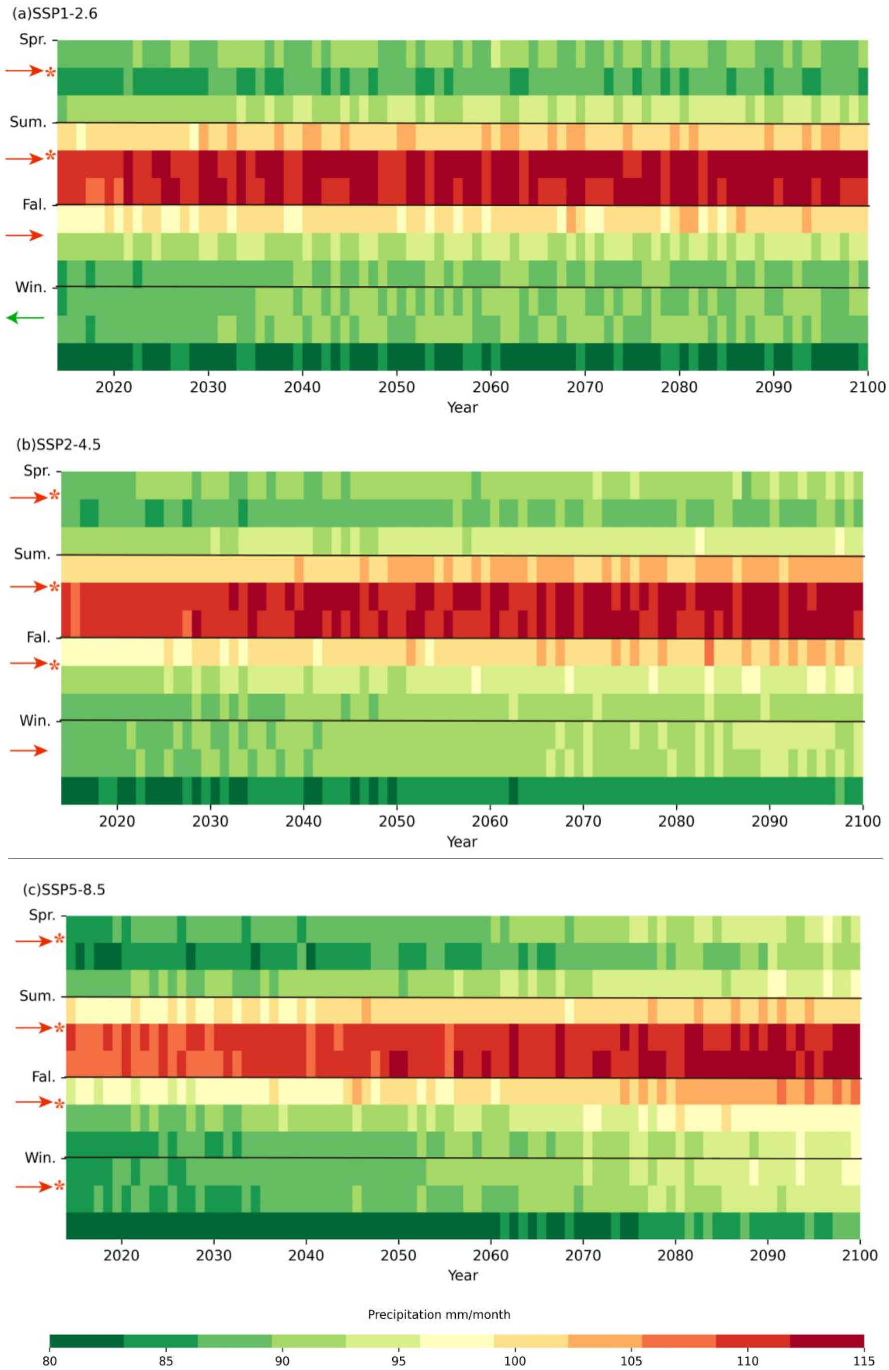

Fig. 9. Mean precipitation changes of each month for global continents under (a) SSP1-2.6, (b) SSP2-4.5 and (c) SSP5-8.5. Each cell represents monthly mean precipitation. Each row is sorted by spring (March to May), summer (June to August),

https://doi.org/10.5194/hess-2022-235
Preprint. Discussion started: 6 July 2022

Hydrology and Earth System Sciences
Open Access
Discussions

fall (September to October) and winter (December to February). The green arrow turning left denotes downward trend, while red arrow facing right denotes upward tendency. Asterisk represents significance value with $p<0.05$.

According to the abundance of precipitation, South America can be categorized as the extremely rainy continent (Fig. 10a), while other studied continents can be grouped as normally rainy continents (Fig. 10b). In respect of SSP1-2.6 and SSP2-4.5, all studied continents exhibit increasing trends of monthly precipitation. While the largest decreasing trend polarization of uneven precipitation at the continental scale under SSP5-8.5 was further detected, suggesting SSP5-8.5 may cause floods or droughts. Asia and Africa which can be classified as precipitation-deficit continents tend to be drier from 2015-2100(p < 0.05) with 19.7% and 15.2% decreasing trends. What's more, South America will be more humid with as the most abundant precipitation continent. Similarly, Europe and North America with relatively abundant precipitation will also usher in more precipitation under SSP5-8.5. To assess the wetting trend of continents more intuitively, the precipitation increases by 7.62%, 15.5% and 6.72% in Europe, North America and South America continents, respectively, while the upward trend is not obvious in Oceania continent.

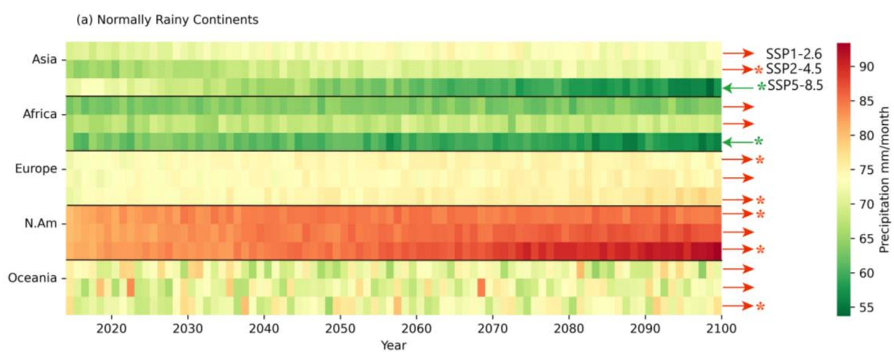

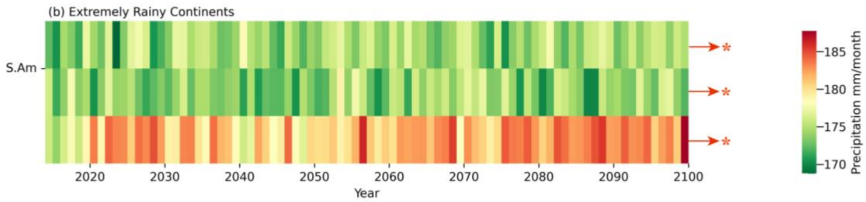

Fig. 10. Land mean rainfall changes of (a) normally rainy continents (Asia, Africa, Europe, N. Am (North America) and Oceania) and (b) extremely rainy continent: S. Am (South America). Each cell represents a monthly mean precipitation value of the continent land. The order of rows is SSP1-2.6, SSP2-4.5 and SSP5-8.5 for each continent. The green arrow turning left denotes downward trend, while red arrow facing right denotes upward tendency. Asterisk (*) represents significance value with $p<0.05$

4. Discussion

4.1 Higher credibility of the proposed ensemble dataset by comparison with previous studies

Majority of previous studies were based on CMIP5 to predict future temperature and precipitation for evaluating ecological impacts of climatic dynamics (Miao et al., 2014; Navarro-Racines et al., 2020; Putra et al., 2020; Kajtar et al., 2021;Tang et al., 2021; Wu et al., 2021). More skillful dataset can improve the spatial correlation accuracy and reduce the bias over the studied region. CMIP6 GCMs with higher resolutions and human activity simulation conditions have been proved with better performance in characterizing the completion processes of carbon emissions, radiative forcing and warming projection (Xin et al., 2020; Zamani et al., 2020; McCrystall et al., 2021; Song et al., 2021). The newly released CMIP6 GCMs were selected to simulate in this study. Besides the new alternation of data sources, there is further improvement of ensemble methods. To decrease the discrepancy between simulation and observation for higher

https://doi.org/10.5194/hess-2022-235
Preprint. Discussion started: 6 July 2022

accuracy, traditional methods (e.g., multi-model ensemble mean, best fitting single model selection) were applied (Rivera and Arnould., 2020; Baker et al., 2021; Kajtar et al., 2021). It is noteworthy that traditional procedure lacks flexibility and ignores the weight allocation of time dimensions. Studies have demonstrated that deep learning can reproduce data in pattern coupling with excellent performance (Sun and Archibald,. 2021; Wei et al., 2021). In this study, considering temporal variation, the application of neural network and machine learning reproduce dataset with higher ability of projecting climatological rainfall and temperature under SSP1-2.6, SSP2-4.5 and SSP5-8.5. Detailed assessment was conducted to find that three new methods are more faultless than any single model. In terms of temperature (precipitation), MAE of proposed dataset reduced from 4.4 ℃ (46.6 mm/month) to 2.1 ℃ (27.3 mm/month) compared with single GCM data.

4.2 Aggravation of global warming and precipitation extreme by socio-economic pathways

The RCP scenarios adopted in CMIP5 were labelled for the range of radiative forcing values until 2100 (2.6, 4.5, 6, and 8.5 W·m^{-2}, respectively) (Rao and Garfinkel 2021). However, SSP-RCPs are joined to describe national policies besides radiative forcing during CMIP6 (Liao et al. 2020). There are different results of global warming and precipitation extreme from these two phases, in which it seems more aggravative in CMIP6 than CMIP5 according to the results from this study. Torres et al. (2022) projected temperature for South America and stated that the years related to 1.5 ℃ and

https://doi.org/10.5194/hess-2022-235
Preprint. Discussion started: 6 July 2022

2 °C thresholds were 2027 and 2040 under RCP8.5, while 2023 and 2034 under SSP5-8.5 during CMIP6, respectively in this study, in which temperature increasing quicker in CMIP5 than CMIP6. Additionally, Bokhari et al. (2018) claimed that the mean temperature over South Asia showed an estimated temperature rising of 3.2°C under RCP4.5 until 2050. Compared with the projection conducted by Bokhari et al. (2018), we have noted that Asia will experience an increasing of 4.32 °C under RCP4.5, which is more intensive than the tendency under SSP2-4.5 in the mid-21st century. Moreover, Ongoma et al. (2018) estimated an increasing in temperature at 2.8 °C and 5.4 °C over East Africa under the RCP4.5 and RCP8.5 scenarios until 2100, respectively. Notably, the increasing tendency over Africa in CMIP6 of this study is 3.4 and 6.0 °C under SSP2-4.5 and 5-8.5, respectively, which is acuter than the increment under RCP4.5 and RCP8.5. Thus, global warming seems to be accelerated under the new socio-economic pathways in CMIP6.

In terms of precipitation, Zhu et al. (2021) demonstrated that the annual precipitation over China would increase by 4.4% and 7% in CMIP5, which is weaker than the trends representing 5.3% and 8.6% under corresponding scenarios in CMIP6. Moreover, Sinha et al. (2018) reported the precipitation Florida may experience 5% rising under RCP4.5, which is 3% lower than trends in SSP2-4.5. It can be demonstrated that the changes of temperature rising and precipitation extreme in these studies agree with our findings, which reveals socio-economic pathways could aggravate global warming and precipitation extreme in the 21st centry.

https://doi.org/10.5194/hess-2022-235
Preprint. Discussion started: 6 July 2022

Hydrology and Earth System Sciences Discussions
Open Access

4.3 Implication for climate changing pattern projected from proposed datasets

It is obvious that the severity of climate changes follows the order of SSP5-8.5 > SSP2-4.5 > SSP1-2.6, in which the scenarios represent durable sustainability, intermediate and fossil-fuel driven high emissions, respectively. Under SSP5-8.5 scenario, GDP growth develops at high speed at the cost of high energy intension in the absence of newly proposed climate management policies. Compared with SSP1-2.6 and SSP2-4.5, time periods breakthrough warming targets come in advance under SSP5-8.5. The analysis results imply that we must adopt reasonable climate intervention policies, including through the pursuit of alternative clean energy instead of fossil fuel-driven approaches. This study also indicated that the phenomena that wet regions become wetter while dry regions become drier due to high emissions, is affected by economic development model to a certain extent. Therefore, conversion of economic development patterns is also one of the factors to be considered in drought and flood mitigation measures. In multi-propose ecological projects, hydropower, agricultural irrigation, drought monitoring and land utilization management need credible evaporation evidence (Paredes et al., 2020). The meteorological factors are related to evaporation estimation. (Lu et al., 2021; Tian et al., 2022). Related equations or indexes (e.g., Penman–Monteith, standardized precipitation index and the standardized precipitation evapotranspiration index) can be constructed employing climate variables to project future ecological system changes (Almorox et al., 2018; Pei et al., 2020). The

https://doi.org/10.5194/hess-2022-235
Preprint. Discussion started: 6 July 2022

new ensemble climate dataset is expected to accurately project climate change and its long-term effects of ecology and environment at a global scale.

5. Conclusion

In this study, high credible findings were proposed based on new ensemble CMIP6 ensemble dataset. We applied three machine learning methods (OLS, DT and DNN) to construct new temperature and precipitation projection dataset, simultaneously. After accuracy evaluation, the optimal monthly methods were selected to generate ensemble dataset under SSP1-2.6, SSP2-4.5 and SSP5-8.5 scenarios. The optimal dataset proved to be higher accuracy from five statistic indicators (R, CRMSE, MAE, SD ratio and CRI) than CMIP6 single model. The ensemble dataset owned CRI ranking first and SD ratio closing to 1 in each month. The new temperature dataset displayed perfect simulation (R = 0.99, CRMSE = 0.19 °C, MAE = 2.05 °C) compared with single CMIP6 GCM (0.95 < R < 0.97, 0.25 °C< CRMSE < 0.30 °C, 3.45 °C < MAE < 4.39 °C), while the new ensembled precipitation dataset was higher credible (R = 0.81, CRMSE = 0.61 mm/month, MAE = 27.31 mm/month) than the single CMIP6 GCM (0.59 < R < 0.77, 0.86 mm/month < CRMSE < 1.1 mm/month, 39.7 mm/month < MAE < 46.57 mm/month).

High credibility findings were conducted depending on this new dataset. Firstly, the intensity order of temperature rising is SSP5-8.5 > SSP2-4.5 > SSP1-2.6 over a global scale. Aisa, Europe and North America continents contributed more to global warming than Oceania, Africa and South America continents under studied three SSPs scenarios. Secondly, the global continent breakthrough 1.5 ℃, 2 ℃ and 3 ℃ rising thresholds in 2024, 2031 and 2048, under SSP5-8.5 scenario. Thirdly, precipitation aggregated during July and August over the global region. April and September to subsequent February can be categorized as dry months under selected SSPs. Fourthly, the ensembled dataset implicates that SSP5-8.5 scenario will accelerate global precipitation polarization (p < 0.05). Precipitation changes in Africa and Asia will decrease, meanwhile, Europe, Oceania and South America will be wetter under the SSP5-8.5 scenario. Associated with former studies, our findings proved that socio-economic pathways could boost global warming and precipitation extreme.

6. Data availability

The CMIP6 GCMs can be downloaded at https://esgf-node.llnl.gov /search/cmip6/. CRU TS4.05 dataset is available at https://crudata.uea.ac.uk/cru/data/hrg/cru_ts_4.05/. The ensemble global new dataset can be accessed via open community Zenodo at https://doi.org/10.5281/zenodo.6565574 (Lu and Zhang, 2022).

Acknowledgments

This work was funded by the National Key Research and Development Program (2018YFC1506506), the Frontier Project of Applied Foundation of Wuhan (2019020701011502), Key Research and Development Program of Jiangxi Province

(20201BBG71002), the ESA-MOST Dragon Program, and the LIESMARS Special Research Funding.

Conflict of interest

The authors declared that there is no conflict of interest.

References

Almazroui, M., Saeed, F., Saeed, S., Ismail, M., Ehsan, M.A., Islam, M.N., Abid, M.A., O'Brien, E., Kamil, S., Rashid, I.U. and Nadeem, I.: Projected Changes in Climate Extremes Using CMIP6 Simulations Over SREX Regions. Earth Systems and Environment, 5, 481-497, 2021.

Almorox, J., Senatore, A., Quej, V.H. and Mendicino, G.: Worldwide assessment of the Penman–Monteith temperature approach for the estimation of monthly reference evapotranspiration. Theoretical and Applied Climatology, 131, 693-703, 2018.

Anthony, K.R.N.: Coral Reefs Under Climate Change and Ocean Acidification: Challenges and Opportunities for Management and Policy. Annual Review of Environment and Resources, 41, 59-81, 2016.

Asuero, A.G., Sayago, A. and González, A.G.: The Correlation Coefficient: An Overview. Critical Reviews in Analytical Chemistry, 36, 41-59, 2006.

Bai, H., Xiao, D., Wang, B., Liu, D.L., Feng, P., and Tang, J.: Multi-model ensemble of CMIP6 projections for future extreme climate stress on wheat in the North China Plain. International Journal of Climatology, 41, E171-E186, 2021.

Baker, J., Souza, D., Kubota, P., Buermann, W., Coelho, C., Andrews, M., Gloor, M., Garcia-Carreras, L., Figueroa, S. and Spracklen, D.: An Assessment of Land–Atmosphere Interactions over South America Using Satellites, Reanalysis, and Two Global Climate Models. Journal of Hydrometeorology, 22, 2021.

Bokhari, S.A.A., Ahmad, B., Ali, J., Ahmad, S., Mushtaq, H.and Rasul, G.: Future climate change projections of the Kabul River Basin using a multi-model ensemble of high-resolution statistically downscaled data. Earth Systems and Environment, 2, 477-497, 2018.

Chen, C.-A., Hsu, H.-H. and Liang, H.-C.: Evaluation and comparison of CMIP6 and CMIP5 model performance in simulating the seasonal extreme precipitation in the Western North Pacific and East Asia. Weather and Climate Extremes, 31, 100303, 2021.

Condro, A.A., Prasetyo, L.B., and Rushayati, S.B.: Short-term projection of Bornean orangutan spatial distribution based on climate and land cover change scenario. In,

https://doi.org/10.5194/hess-2022-235
Preprint. Discussion started: 6 July 2022

Hydrology and Earth System Sciences Discussions

Sixth International Symposium on LAPAN-IPB Satellite (p. 113721B): International Society for Optics and Photonics, 2019.

Dar, J. and Dar, A.Q.: Spatio-temporal variability of meteorological drought over India with footprints on agricultural production. Environmental Science and Pollution Research, 28, 55796-55809, 2021.

Das, L., Meher, J.K. and Dutta, M.: Construction of rainfall change scenarios over the Chilka Lagoon in India. Atmospheric Research, 182, 36-45, 2016.

Fu, Y., Lin, Z. and Guo, D.: Improvement of the simulation of the summer East Asian westerly jet from CMIP5 to CMIP6. Atmospheric and Oceanic Science Letters, 13, 550-558, 2020.

Gaitán, E., Monjo, R., Pórtoles, J. and Pino-Otín, M.R.: Projection of temperatures and heat and cold waves for Aragón (Spain) using a two-step statistical downscaling of CMIP5 model outputs. Science of The Total Environment, 650, 2778-2795, 2019.

Gianinetto, M., Aiello, M., Vezzoli, R., Polinelli, F.N., Rulli, M.C., Chiarelli, D.D., Bocchiola, D., Ravazzani, G. and Soncini, A.: Future scenarios of soil erosion in the Alps under climate change and land cover transformations simulated with automatic machine learning. Climate, 8, 28, 2020.

Hamed, M.M., Nashwan, M.S., Shahid, S., Ismail, T.b., Wang, X.-j., Dewan, A. and Asaduzzaman, M. :Inconsistency in historical simulations and future projections of temperature and rainfall: A comparison of CMIP5 and CMIP6 models over Southeast Asia. Atmospheric Research, 265, 105927, 2022.

Hermans, T.H., Gregory, J.M., Palmer, M.D., Ringer, M.A., Katsman, C.A. and Slangen, A.B.: Projecting global mean sea-level change using CMIP6 models. Geophysical Research Letters, 48, e2020GL092064, 2021.

Hulme, M.: 1.5 °C and climate research after the Paris Agreement. Nature Climate Change, 6, 222-224,2016.

IPCC, 2021: Climate Change 2021: The Physical Science Basis. Contribution of Working Group I to the Sixth Assessment Report of the Intergovernmental Panel on Climate Change[Masson-Delmotte, V., P. Zhai, A. Pirani, S.L. Connors, C. Péan, S. Berger, N. Caud, Y. Chen, L. Goldfarb, M.I. Gomis, M. Huang, K. Leitzell, E. Lonnoy, J.B.R. Matthews, T.K. Maycock, T. Waterfield, O. Yelekçi, R. Yu, and B. Zhou (eds.)]. Cambridge University Press, Cambridge, United Kingdom and New York, NY, USA, In press, doi:10.1017/9781009157896.

Iqbal, Z., Shahid, S., Ahmed, K., Ismail, T., Ziarh, G.F., Chung, E.-S. and Wang, X.: Evaluation of CMIP6 GCM rainfall in mainland Southeast Asia. Atmospheric Research, 254, 105525, 2021.

Iwamura, T., Guzman-Holst, A. and Murray, K.A.: Accelerating invasion potential of disease vector Aedes aegypti under climate change. Nature Communications, 11, 2130, 2020.

Jiang, H., Lu, N., Qin, J., Tang, W. and Yao, L.: A deep learning algorithm to estimate hourly global solar radiation from geostationary satellite data. Renewable and Sustainable Energy Reviews, 114, 109327, 2019.

Jiang, H., Lu, N., Qin, J. and Yao, L.: Surface global and diffuse solar radiation over

https://doi.org/10.5194/hess-2022-235
Preprint. Discussion started: 6 July 2022

China acquired from geostationary Multi-functional Transport Satellite data. Earth Syst. Sci. Data Discuss., 1-22, 2019.

Jiang, Z., Li, W., Xu, J. and Li, L.: Extreme Precipitation Indices over China in CMIP5 Models. Part I: Model Evaluation. Journal of Climate, 28, 8603-8619, 2015.

Jose, D.M., Vincent, A.M. and Dwarakish, G.S.: Improving multiple model ensemble predictions of daily precipitation and temperature through machine learning techniques. Scientific Reports, 12, 1-25, 2022.

Jumin, E., Basaruddin, F.B., Yusoff, Y.B.M., Latif, S.D. and Ahmed, A.N.: Solar radiation prediction using boosted decision tree regression model: A case study in Malaysia. Environmental Science and Pollution Research, 28, 26571-26583, 2021.

Kajtar, J.B., Santoso, A., Collins, M., Taschetto, A.S., England, M.H. and Frankcombe, L.M.: CMIP5 intermodel relationships in the baseline Southern Ocean climate system and with future projections. Earth's Future, 9, e2020EF001873, 2021.

Kuma, P., Bender, F.A.-M., Schuddeboom, A., McDonald, A.J. and Seland, Ø.: Machine learning of cloud types shows higher climate sensitivity is associated with lower cloud biases. Atmospheric Chemistry and Physics Discussions, 1-32, 2022.

Lee, J., Lee, W.S., Jung, H. and Lee, S.-G.: Comparison between total least squares and ordinary least squares in obtaining the linear relationship between stable water isotopes. Geoscience Letters, 9, 11, 2022.

Lee, Y., Paek, J., Park, J.-S. and Boo, K.-O.: Changes in temperature and rainfall extremes across East Asia in the CMIP5 ensemble. Theoretical and Applied Climatology, 141, 143-155, 2022.

Li, C., Lu, Y., Liu, J., & Wu, X.: Climate change and dengue fever transmission in China: Evidences and challenges. Science of The Total Environment, 622-623, 493-501, 2018.

Li, S.-Y., Miao, L.-J., Jiang, Z.-H., Wang, G.-J., Gnyawali, K.R., Zhang, J., Zhang, H., Fang, K., He, Y., and Li, C.: Projected drought conditions in Northwest China with CMIP6 models under combined SSPs and RCPs for 2015–2099. Advances in Climate Change Research, 11, 210-217, 2020.

Liao, W., Liu, X., Xu, X., Chen, G., Liang, X., Zhang, H. and Li, X.: Projections of land use changes under the plant functional type classification in different SSP-RCP scenarios in China. Science Bulletin, 65, 1935-1947, 2020.

Liu, M., and Grana, D.: Accelerating geostatistical seismic inversion using TensorFlow: A heterogeneous distributed deep learning framework. Computers & Geosciences, 124, 37-45, 2019.

Lu, J., Wang, G., Chen, T., Li, S., Hagan, D.F.T., Kattel, G., Peng, J., Jiang, T. and Su, B.: A harmonized global land evaporation dataset from model-based products covering 1980–2017. Earth Syst. Sci. Data, 13, 5879-5898, 2021.

Lu, J., and Zhang, P.: EPTGODD-WHU: Ensemble Precipitation and Temperature from CMIP6 GCMs optimized by OLS-DT-DNN methods integration (1850-2100) (Version 1.0) [Data set]. Zenodo, https://doi.org/10.5281/zenodo.6565574, 2022.

Liu, Z., Lu, J., Huang, J., Chen, X. and Zhang, L.: Projection of reference crop evapotranspiration under future climate change in Poyang Lake Watershed, China.

https://doi.org/10.5194/hess-2022-235
Preprint. Discussion started: 6 July 2022

Journal of Hydrologic Engineering 26(1): 05020042, 2021.

Maimon, Z., Raveh, A. and Mosheiov, G.: Additional cautionary notes about the Pearson's correlation coefficient. Quality and Quantity, 20, 313-325, 1986.

Mitra, A.: A Comparative Study on the Skill of CMIP6 Models to Preserve Daily Spatial Patterns of Monsoon Rainfall Over India. Frontiers in Climate, 3, 2021.

McCrystall, M.R., Stroeve, J., Serreze, M., Forbes, B.C. and Screen, J.A.: New climate models reveal faster and larger increases in Arctic precipitation than previously projected. Nature Communications, 12, 6765, 2021.

Miao, C., Duan, Q., Sun, Q., Huang, Y., Kong, D., Yang, T., Ye, A., Di, Z. and Gong, W.: Assessment of CMIP5 climate models and projected temperature changes over Northern Eurasia. Environmental Research Letters, 9, 055007, 2014.

Narsey, S., Brown, J., Colman, R., Delage, F., Power, S., Moise, A. and Zhang, H.: Climate change projections for the Australian monsoon from CMIP6 models. Geophysical Research Letters, 47, e2019GL086816, 2020.

Navarro-Racines, C., Tarapues, J., Thornton, P., Jarvis, A. and Ramirez-Villegas, J.: High-resolution and bias-corrected CMIP5 projections for climate change impact assessments. Scientific Data, 7, 7, 2020.

O'Neill, B.C., Tebaldi, C., van Vuuren, D.P., Eyring, V., Friedlingstein, P., Hurtt, G., Knutti, R., Kriegler, E., Lamarque, J.F., Lowe, J., Meehl, G.A., Moss, R., Riahi, K. and Sanderson, B.M.: The Scenario Model Intercomparison Project (ScenarioMIP) for CMIP6. Geosci. Model Dev., 9, 3461-3482, 2016.

O'Neill, B.C., Kriegler, E., Ebi, K.L., Kemp-Benedict, E., Riahi, K., Rothman, D.S., van Ruijven, B.J., van Vuuren, D.P., Birkmann, J. and Kok, K. The roads ahead: Narratives for shared socioeconomic pathways describing world futures in the 21st century. Global environmental change, 42, 169-180, 2017.

Ongoma, V., Chen, H. and Gao, C.: Projected changes in mean rainfall and temperature over East Africa based on CMIP5 models. International Journal of Climatology, 38, 1375-1392, 2018.

Ortiz-Bobea, A., Ault, T.R., Carrillo, C.M., Chambers, R.G. and Lobell, D.B.: Anthropogenic climate change has slowed global agricultural productivity growth. Nature Climate Change, 11, 306-312, 2021.

Paredes, P., Pereira, L.S., Almorox, J. and Darouich, H.: Reference grass evapotranspiration with reduced data sets: Parameterization of the FAO Penman-Monteith temperature approach and the Hargeaves-Samani equation using local climatic variables. Agricultural Water Management, 240, 106210, 2020.

Pei, Z., Fang, S., Wang, L. and Yang, W.: Comparative Analysis of Drought Indicated by the SPI and SPEI at Various Timescales in Inner Mongolia, China. Water, 12, 2020.

Pekel, E.: Estimation of soil moisture using decision tree regression. Theoretical and Applied Climatology, 139, 1111-1119, 2020.

Putra, I.D., Rosid, M., Sopaheluwakan, A. and Sianturi, Y.: The CMIP5 projection of extreme climate indices in Indonesia using simple quantile mapping method, AIP Conference Proceedings 2223, 050008. https://doi.org/10.1063/5.0000849. 2020.

Qi, W., Feng, L., Yang, H., Zhu, X., Liu, Y. and Liu, J.: Weakening flood, intensifying

https://doi.org/10.5194/hess-2022-235
Preprint. Discussion started: 6 July 2022

hydrological drought severity and decreasing drought probability in Northeast China. Journal of Hydrology: Regional Studies, 38, 100941, 2021.

Raheli, B., Aalami, M.T., El-Shafie, A., Ghorbani, M.A. and Deo, R.C.: Uncertainty assessment of the multilayer perceptron (MLP) neural network model with implementation of the novel hybrid MLP-FFA method for prediction of biochemical oxygen demand and dissolved oxygen: a case study of Langat River. Environmental Earth Sciences, 76, 503, 2017.

Randall, C.J. and van Woesik, R.: Contemporary white-band disease in Caribbean corals driven by climate change. Nature Climate Change, 5, 375-379, 2015.

Rao, J., and Garfinkel, C.I: CMIP5/6 models project little change in the statistical characteristics of sudden stratospheric warmings in the 21st century. Environmental Research Letters, 16, 034024, 2021.

Raupach, T.H., Martius, O., Allen, J.T., Kunz, M., Lasher-Trapp, S., Mohr, S., Rasmussen, K.L., Trapp, R.J. and Zhang, Q.: The effects of climate change on hailstorms. Nature Reviews Earth & Environment, 2, 213-226, 2021.

Rivera, J.A. and Arnould, G.: Evaluation of the ability of CMIP6 models to simulate precipitation over Southwestern South America: Climatic features and long-term trends (1901–2014). Atmospheric Research, 241, 104953, 2020.

Sanderson, B.M., Knutti, R. and Caldwell, P.: Addressing interdependency in a multimodel ensemble by interpolation of model properties. Journal of Climate, 28, 5150-5170, 2015.

Schleussner, C.-F., Rogelj, J., Schaeffer, M., Lissner, T., Licker, R., Fischer, E.M., Knutti, R., Levermann, A., Frieler, K. and Hare, W.: Science and policy characteristics of the Paris Agreement temperature goal. Nature Climate Change, 6, 827-835, 2016.

Sharif, B., Makowski, D., Plauborg, F. and Olesen, J.E.: Comparison of regression techniques to predict response of oilseed rape yield to variation in climatic conditions in Denmark. European Journal of Agronomy, 82, 11-20, 2017.

Sinha, P., Mann, M.E., Fuentes, J.D., Mejia, A., Ning, L., Sun, W., He, T. and Obeysekera, J.: Downscaled rainfall projections in south Florida using self-organizing maps. Science of The Total Environment, 635, 1110-1123, 2018.

Singh, S., Ghosh, S., Sahana, A., Vittal, H. and Karmakar, S.: Do dynamic regional models add value to the global model projections of Indian monsoon? Climate Dynamics, 48, 1375-1397, 2017.

Song, Y.H., Nashwan, M.S., Chung, E.-S., & Shahid, S.: Advances in CMIP6 INM-CM5 over CMIP5 INM-CM4 for precipitation simulation in South Korea. Atmospheric Research, 247, 105261, 2021.

Sun, Z. and Archibald, A.T.: Multi-stage ensemble-learning-based model fusion for surface ozone simulations: A focus on CMIP6 models. Environmental Science and Ecotechnology, 8, 100124, 2021.

Tang, T., Luo, J.-J., Peng, K., Qi, L. and Tang, S.: Over-projected Pacific warming and extreme El Niño frequency due to CMIP5 common biases. National science review, 8, nwab056, 2021.

Taylor, K.: Summarizing multiple aspects of model performance in a single diagram.

Journal of Geophysical Research, 106, 7183-7192, 2001.
Tian, Q., Lu, J. and Chen, X.: A novel comprehensive agricultural drought index reflecting time lag of soil moisture to meteorology: A case study in the Yangtze River basin, China. CATENA, 209, 105804, 2022.
Torres, R.R., Benassi, R.B., Martins, F.B. and Lapola, D.M.: Projected impacts of 1.5 and 2 C global warming on temperature and precipitation patterns in South America. International Journal of Climatology, 42, 1597-1611, 2022.
Tran Anh, D., Van, S.P., Dang, T.D. and Hoang, L.P.: Downscaling rainfall using deep learning long short-term memory and feedforward neural network. International Journal of Climatology, 39, 4170-4188, 2019.
Ullah, S., You, Q., Zhang, Y., Bhatti, A.S., Ullah, W., Hagan, D.F.T., Ali, A., Ali, G., Jan, M.A., Khan, S.N. and Ali, A.: Evaluation of CMIP5 models and projected changes in temperatures over South Asia under global warming of 1.5 oC, 2 oC, and 3 oC. Atmospheric Research, 246, 105122, 2020.
Vandal, T., Kodra, E. and Ganguly, A.R.: Intercomparison of machine learning methods for statistical downscaling: the case of daily and extreme precipitation. Theoretical and Applied Climatology, 137, 557-570, 2019.
Wei, X., Wang, G., Feng, D., Duan, Z., Hagan, D.F.T., Tao, L., Miao, L., Su, B. and Jiang, T: Deep-Learning-Based Harmonization and Super-Resolution of Near-Surface Air Temperature from CMIP6 Models (1850-2100). Earth Syst. Sci. Data Discuss., 1-27, 2021.
Wu, C., Yeh, P.J.-F., Chen, Y.-Y., Lv, W., Hu, B.X. and Huang, G.: Copula-based risk evaluation of global meteorological drought in the 21st century based on CMIP5 multi-model ensemble projections. Journal of Hydrology, 598, 126265, 2021.
Xin, X., Wu, T., Zhang, J., Yao, J. and Fang, Y.: Comparison of CMIP6 and CMIP5 simulations of precipitation in China and the East Asian summer monsoon. International Journal of Climatology, 40, 6423 – 6440, 2020.
Xu, H., Chen, H. and Wang, H.: Future changes in precipitation extremes across China based on CMIP6 models. International Journal of Climatology, 42, 635-651, 2022.
Xu, R., Chen, N., Chen, Y. and Chen, Z: Downscaling and projection of multi-CMIP5 Precipitation using machine learning methods in the upper Han River Basin. Advances in Meteorology, https://doi.org/10.1155/2020/8680436, 2020.
You, Q., Cai, Z., Wu, F., Jiang, Z., Pepin, N. and Shen, S.S.P.: Temperature dataset of CMIP6 models over China: evaluation, trend and uncertainty. Climate Dynamics, 57, 17-35, 2021.
Zamani, Y., Hashemi Monfared, S.A., Azhdari moghaddam, M. and Hamidianpour, M.: A comparison of CMIP6 and CMIP5 projections for precipitation to observational data: the case of Northeastern Iran. Theoretical and Applied Climatology, 142, 1613-1623, 2020.
Zhang, L., Chen, X., Lu, J., Fu, X., Zhang, Y., Liang, D. and Xu, Q.: Precipitation projections using a spatiotemporally distributed method: a case study in the Poyang Lake watershed based on the MRI-CGCM3. Hydrology and Earth System Sciences, 23, 1649-1666, 2019.
Zhu, H., Jiang, Z., Li, J., Li, W., Sun, C. and Li, L.: Does CMIP6 Inspire More

https://doi.org/10.5194/hess-2022-235
Preprint. Discussion started: 6 July 2022

Hydrology and Earth System Sciences
Discussions

830 Confidence in Simulating Climate Extremes over China? Advances in
831 Atmospheric Sciences, 37, 1119-1132, 2020.